ENCLOSURE 2

Non-Proprietary Transnuclear Calculation 972-179, Revision 0, T-68 High Burnup Cladding Mechanical Properties, November 2004

Calvert Cliffs Nuclear Power Plant, LLC
September 1, 2010

TRANSNUCLEAR An AREVA Company	Form 3.2-1 Calculation Cover Sheet	Calc. No.:	972-179		
		Rev. No.:	0		
Calculation Title: TN-68 High Burnup Cladding Mechanical Properties		Page:	1	of	13
		Project No.:	60972		
		DCR No.:			

Project Name: TN-68 High Burnup Transport

Number of CDs attached:

If original issue, is Licensing Review per TIP 3.5 required?

☒ No (explain)	☐ Yes	Licensing Review No._____

TN-68 High Burnup is under development and is not yet licensed.

Software utilized: N/A Version: N/A

Calculation is complete

Originator's Signature:	S. Streutker	Date: 11/04/05

Calculation has been checked for consistency, completeness, and correctness

Checker Signature:	P. Shih	Date: 11/04/05

Calculation is approved for use

Project Engineer Signature:	W. Bracy	Date: 11/9/05

1.0 Purpose

The purpose of this calculation is to provide material properties, modulus of elasticity and yield stress, for spent fuel cladding. These values will be supplied for both Zircaloy-2 and Zircaloy-4 over a range of temperatures, 300 °F to 750 °F. These values are to be used in structural calculations that determine the ability of the spent fuel rods to withstand regulatory drop accidents.

2.0 References

[redacted]

Proprietary Information with Pursuant to 10CFR 2.390

3. Chun, R., M. Witte, M. Schwarz, *Dynamic Impact Effects on Spent Fuel Assemblies,* October, 1987, pp. 3.

4. TN calculation NUH24PTH.0406, "Thermal Expansion of 24PTH DSC Basket Components and Irradiated Fuel Assembly Within DSC Cavity", Rev. 0.

3.0 Methodology and Assumptions

The expressions used to determine the material properties are taken from Ref. 1. These expressions were derived from correlations of experimental results of several different investigations. Unless otherwise noted, all input values are taken from Ref. 1.

Temperature is a significant factor in derivation of Zircaloy properties. These properties are calculated over a range of temperatures for both Zircaloy-4 and Zircaloy-2. Example calculations will be carried out below for Zircaloy-4 (PWR cladding) and Zircaloy-2 (BWR cladding) at 750°F.

[redacted]

Proprietary Information with Pursuant to 10CFR 2.390

[redacted]

Proprietary Information with
Pursuant to 10CFR 2.390

4.0 Zircaloy-4 (PWR) Calculations

[redacted]

Proprietary Information with
Pursuant to 10CFR 2.390

[redacted]

Proprietary Information with
Pursuant to 10CFR 2.390

[redacted]

Proprietary Information with
Pursuant to 10CFR 2.390

[redacted]

Proprietary Information with
Pursuant to 10CFR 2.390

5.0 Zircaloy-2 (BWR) Calculations

[redacted]

Proprietary Information with
Pursuant to 10CFR 2.390

[redacted]

Proprietary Information with
Pursuant to 10CFR 2.390

[redacted]

Proprietary Information with
Pursuant to 10CFR 2.390

6.0 Results

The expressions above have been used to calculate the modulus of elasticity, E and the Yield Stress, σ_y over a range of temperatures. The results for both Zircaloy-4 (PWR) and Zircaloy-2 (BWR) are presented in Table 1 and Figures 1 and 2 below.

Table 1 Modulus of Elasticity and Yield Stress (0.5 s^{-1} strain rate)

[redacted]

Proprietary Information with
Pursuant to 10CFR 2.390

[redacted]

Proprietary Information with
Pursuant to 10CFR 2.390

[redacted]

Proprietary Information with
Pursuant to 10CFR 2.390

Appendices

Appendix 1 - PNNL STRESS/STRAIN CORRELATION FOR ZIRCALOY

Appendix 2 - [redacted] Proprietary Information with Pursuant to 10CFR 2.390

APPENDIX 1

PNNL STRESS/STRAIN CORRELATION FOR ZIRCALOY

K. J. Geelhood and C.E. Beyer
Pacific Northwest National Laboratory
March 2005

PNNL Stress/Strain Correlation for Zircaloy

1. Introduction

Pacific Northwest National Laboratory (PNNL) was tasked with incorporating cladding mechanical property data into the Nuclear Regulatory Commission (NRC) fuel codes, FRAPCON-3[1] and FRAPTRAN[2] by NRC Office of Nuclear Reactor Research. The data used in this effort is all of the data that was available to PNNL at the beginning of June, 2004. The data that was available includes a database of mechanical properties that has been compiled by PNNL, and recently expanded. This database consists of yield and ultimate tensile strengths, uniform and total strain, local fast fluence, local burnup, corrosion level, hydrogen concentrations, test temperature, strain rate, and cold work ratio for each specimen. Information on cold-work level is many times not expressly given and, therefore, was estimated from information provided on fabrication. This data comes from the open literature and some proprietary sources. Other available data come from the PROMETRA program and consists of high burnup cladding yield and ultimate tensile strengths as a function of temperature and strain rate with limited information on corrosion and hydrogen levels. It should be noted that the PROMETRA data are not included in the PNNL database because the data are only plotted on a figure from a limited distribution report. The data from Argonne National Laboratory (ANL) was not available to PNNL at the beginning of June, 2004, so it was not used in this effort.

The objective of this task is to create a mechanical model that can calculate true stress, and true strain, and possible failure of the fuel rod cladding based on uniaxial test data. The mechanical models fitted coefficients are based on data from uniaxial tests (or biaxial tests normalized to a uniaxial stress state) that measure yield strength, ultimate tensile strength and uniform elongation as well as engineering stress/strain curves when available.

The PNNL database of yield strength, ultimate tensile strength and uniform elongation consists of approximately 200 uniaxial tube tension tests[3-18], 150 biaxial burst tests[1-3, 6, 7, 8], and 130[6, 8, 12, 13, 22-24] ring stretch tests. The temperature, strain rate, and fast fluences of this data ranged from 293K to 673K, 4×10^{-3} to 2×10^{-6} /s, and 0.0 to 1.26×10^{26} n/m^2, respectively. The data from References 6 and 9 have recently been added to this database. The PROMETRA database[25] from Commissariat à l'Energie Atomique (CEA) consists of 105 ring stretch and axial tension tests on cladding over the temperature, strain rate, and fast fluence ranges of 293K to 1273K, 0.01 to 5 /s, and 6×10^{25} to 1.2×10^{26}n/m^2, respectively. However, PNNL only has a plot of these data as a function of temperature abd does not have a tabulation of each individual data point. As a result, the PROMETRA data are not tabulated in the PNNL database. The PROMETRA data were used to determine the strain rate and temperature dependence on above 4×10^{-3} /s and 673K because these data are lacking in the PNNL database.

The uniaxial tension test data from the PNNL database will be used directly as measured, since these tests are for a uniaxial stress state, i.e., $\sigma_2 = \sigma_3 = 0$. The biaxial burst test data from the PNNL database will be adjusted down by multiplying by a factor of $\sqrt{3}/2$

as predicted by the von Misses failure criteria[26] for this biaxial stress state, where $\sigma_1=2\sigma_2$. The ring test data can be used as measured, however, it has been demonstrated that a large degree of scatter exists in the strain data from ring tests, particularly when comparing data taken from different labs. It was decided that the scatter in the ring test data in the PNNL database may be too great to be used in model fitting. However, the ring test yield stress and ultimate tensile strength data were compared to the final models for yield stress and ultimate tensile strength and were found to fit as well as the axial and burst test data used to fit these models.

2. Model Description

The stress vs. strain behavior of Zircaloy is described by two different correlations, depending on the stress, Before yield, Hooke's law, as seen in Equation 1 is used to describe the elastic deformation of the Zircaloy.

$$\sigma = \varepsilon \cdot E \qquad \text{(Equation 1)}$$

where:

σ = stress

ε = strain

E = elastic modulus

After yield, the power law, as seen in Equation 2 is used to describe the plastic deformation of the Zircaloy.

$$\sigma = K \cdot \varepsilon^n \left(\frac{\dot{\varepsilon}}{10^{-3}} \right)^m \qquad \text{(Equation 2)}$$

where:

K = strength coefficient

n = strain hardening exponent

m = strain rate exponent

$\dot{\varepsilon}$ = strain rate, s^{-1}

The yield stress is given as the non-zero intersection of Equations 1 and 2. The intersection of these equations is given in Equation 3.

$$\sigma_y = \left[\frac{K}{E^n} \left(\frac{\dot{\varepsilon}}{10^{-3}} \right)^m \right]^{\left(\frac{1}{1-n}\right)} \qquad \text{(Equation 3)}$$

The ultimate tensile strength can be approximated by the stress predicted by Equation 2, when the strain is the sum of the plastic strain at maximum load and the strain at yield, σ_y/E. The plastic strain at maximum load it typically referred to as, uniform elongation (UE), by the fuel vendors. In this report the quantity describing the plastic strain at maximum load will be referred to as uniform elongation. A sample true stress vs. true strain curve can be seen in Figure 1. In this figure, the true stress strain behavior that is predicted by the model can be seen. The two parts, elastic and plastic, that make up this curve, as described above, can also be seen.

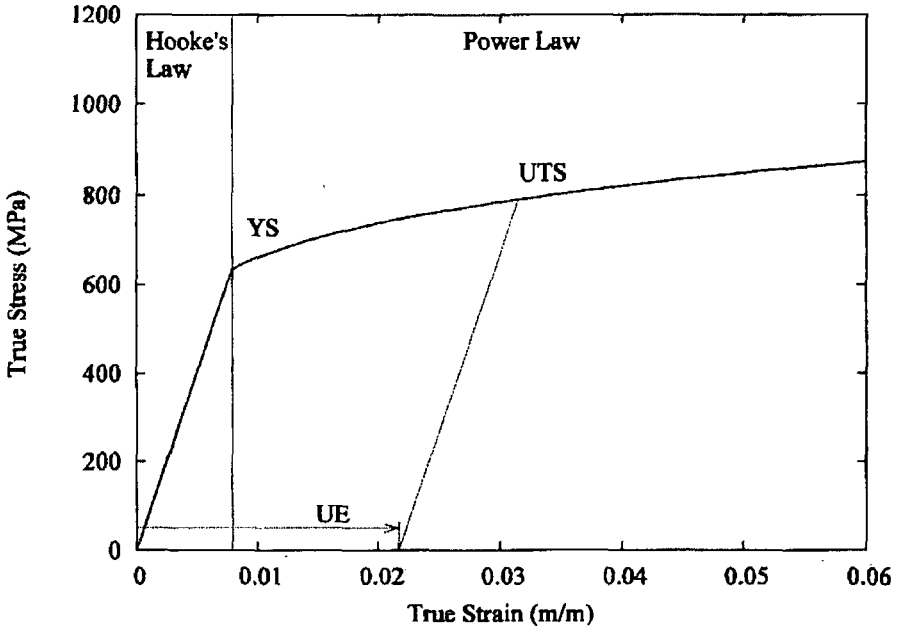

Figure 1: Sample stress vs. strain curve using new model

Empirical models for E, K, n, m, and UE were developed and are described in detail below.

2.1 Elastic Modulus

The elastic modulus of Zircaloy that was used in this model is the same model that is given in MAPTRO-11[27]. The description of this model is given below.

$$E = \frac{1.088\times10^{11} - 5.475\times10^{7}\cdot T + K_1 + K_2}{K_3} \qquad T\leq 1090K$$

$$E = \left(E(1255) - E(1090)\right)\frac{T-1090}{1255-1090} + E(1090) \qquad 1090K<T<1255\ K$$

$$E = 9.21\times10^{10} - 4.05\times10^{7}\cdot T \qquad T\geq 1255\ K$$

where:

E = elastic modulus, Pa

T = temperature, K

$K_1 = (6.61\times10^{11} + 5.912\times10^{8}\cdot T)\Delta$

Δ = average oxygen concentration minus oxygen concentration of as-received cladding (kg oxygen/kg Zircaloy)

$K_2 = -2.6\times10^{10}\cdot CW$

CW= cold work, unitless ratio of areas (valid from 0 to 0.75)

$K_3 = 0.88 + 0.12\exp(-\Phi/10^{25})$

Φ = fast neutron fluence, n/m^2

2.2 Strength Coefficient

The strength coefficient, K, is a function of temperature, fast neutron fluence, cold work, and alloy composition. The models for the strength coefficients of Zircaloy-2 and Zircaloy-4 are given below.

$$K = K(T)\cdot(1 + K(CW) + K(\Phi))/K(Zry)$$

Where:

K = strength coefficient, Pa

$$K(T) = 1.17628\times10^{9} + 4.54859\times10^{5}T - 3.28185\times10^{3}T^{2} + 1.72752\cdot T^{3} \quad T<750K$$

$$K(T) = 2.522488\times10^{6}\exp\left(\frac{2.8500027\times10^{6}}{T^{2}}\right) \quad 750K<T<1090K$$

$$K(T) = 1.841376039\times10^{8} - 1.4345448\times10^{5}T \quad 1090K<T<1255K$$

$$K(T) = 4.330\times10^{7} - 6.685\times10^{4}T + 3.7579\times10^{1}T^{2} - 7.33\times10^{-3}T^{3} \quad 1255K<T<2100K$$

$$K(CW) = 0.546\cdot CW$$

$$K(\Phi) = (-0.1464 + 1.464\times10^{-25}\Phi)f(CW,T) \quad \Phi< 0.1x10^{25}\ n/m^2$$

$$K(\Phi) = 2.928\times10^{-26}\Phi \quad 0.1x10^{25}n/m^2<\Phi< 2x10^{25}\ n/m^2$$

$$K(\Phi) = 0.53236 + 2.6618\times10^{-27}\Phi \quad 2x10^{25}\ n/m^2<\Phi<7.5x10^{25}\ n/m^2$$

$$K(\Phi) = 0.731995 \quad \Phi>7.5x10^{25}\ n/m^2$$

$$f(CW,T) = 2.25\exp(-20\cdot CW)\cdot\min\left[1,\exp\left(\frac{T-550}{10}\right)\right]+1$$

K(Zry)=1 for Zircaloy-4

K(Zry)=1.305 for Zircaloy-2

T = temperature, K

CW= cold work, unitless ratio of areas (valid from 0 to 0.75)

Φ = fast neutron fluence, n/m^2

2.3 Strain Hardening Exponent

The strain hardening exponent, n, is a function of temperature, fast neutron fluence, and alloy composition. The models for the strain hardening exponents of Zircaloy-2 and Zircaloy-4 are given below.

$$n = n(T)\cdot n(\Phi)/n(Zry)$$

where:

n = strain hardening exponent

$$n(T) = 0.11405 \quad T<419.4K$$

$$n(T) = -9.490\times10^{-2} + 1.165\times10^{-3}T - 1.992\times10^{-6}T^{2} + 9.588\times10^{-10}T^{3} \quad 419.4K<T<1099.0772K$$

$$n(T) = -0.22655119 + 2.5\times10^{-4}T \quad 1099.0772K<T<1600K$$

$$n(T) = 0.17344880 \quad T>1600K$$

$$n(\Phi) = 1.321 + 0.48\times10^{-25}\Phi \quad \Phi< 0.1x10^{25}\ n/m^2$$

$$n(\Phi) = 1.369 + 0.096\times10^{-25}\Phi \quad 0.1x10^{25}\ n.m^2<\Phi< 2x10^{25}\ n/m^2$$

$n(\Phi) = 1.5435 + 0.008727 \times 10^{-25} \Phi$ $2x10^{25}$ n/m²<Φ<$7.5x10^{25}$ n/m²

$n(\Phi) = 1.608953$ Φ>$7.5x10^{25}$ n/m²

n(Zry) = 1 for Zircaloy-4
n(Zry) = 1.6 for Zircaloy-2
T = temperature, K
Φ = fast neutron fluence, n/m²

2.4 Strain Rate Exponent

The strain rate exponent, m, is given by a constant value, described in the equation below

$m = 0.015$ T<750K

$m = 7.458 \times 10^{-4} T - 0.544338$ 750K<T<800K

$m = 3.24124 \times 10^{-4} T - 0.20701$ T>800K

Where:
m = strain rate exponent
T = temperature, K

The impact of the strain rate exponent on yield stress is to increase the yield strength with increasing strain rate, but the effect is not large. For example, increasing the strain rate from $1x10^{-4}$ /s to 1.0 /s will increase the yield strength by about 15%.

2.5 Uniform Elongation

The uniform plastic elongation for irradiated Zircaloy is given below. This model can by used for un-irradiated Zircaloy, but there is considerable scatter in the unirradiated data.

$UE = \min(UE_0, UE_{Hex})$

Where:
UE = uniform plastic elongation, %
UE_0= 2.2%

$UE_{Hex} = A \cdot H_{ex}^{-p}$ H_{ex}>0

$UE_{Hex} = UE_0$ H_{ex}=0

$A = 1211 \exp(-0.00927 \cdot T)$ T<700K

$A = 1.840803$ T>700K

$p = 1.355231 - 0.001783 \cdot T$ T<700K

$p = 0.107131$ T>700K

$H_{ex} = \max(0, H_{Tot} - H_{Sol})$

$$H_{Sol} = 1.2 \times 10^5 \exp\left(\frac{-8550}{1.985887 \cdot T}\right)$$

H_{Tot} = total hydrogen in cladding, ppm
T = temperature, K

The excess hydrogen calculated above is found using the steady state hydrogen solubility. In the case of fast transients, the hydrogen takes a finite time to go into solution. In order

to model this time, the hydrogen dissolution and precipitation rates must be modeled as discussed in a separate paper.[28].

3. Data comparisons

This section shows how well the new stress/strain correlation fits to the available data. In this section, the modified yield stress from the burst tests and the measured yield stress from the axial tension tests from the PNNL database and the measured yield stress from the PROMETRA plotted data are compared to the model predictions. The adjusted (adjusted to uniaxial stress) ultimate tensile strength from the burst tests and the measured ultimate tensile strength from the uniaxial tension tests (from the PNNL database) are compared to the model predictions. The uniform elongations from the burst tests and uniaxial tension tests (from the PNNL database) from irradiated samples are compared to the model predictions. The measured stress vs. strain curves up to uniform elongation (from the PNNL database) are compared to the model predictions. Finally the yield stress and ultimate tensile strength from the ring tests (from the PNNL database) are compared with the model predictions.

3.1 Yield Stress

Figure 2 shows a plot of predicted yield stress vs. measured yield stress for burst tests and axial tension tests from the PNNL database. It can be seen from this figure that the model predicts the data quite well. Generally the upper and lower bound in such yield stress data is ±140 MPa, while the model standard error is 66 MPa.

Figures 3, 4, 5, and 6 show the predicted minus measured values for the PNNL database as a function of fluence, cold work, strain rate, and temperature, respectively. It can be seen from these figures that there is no apparent bias as a function of cold work, fluence, strain rate, or temperature. Figure 7 shows the predicted minus measured values for the PNNL database as a function of excess hydrogen. PNNL has not observed any change in yield stress as a function of hydrogen concentration. However, an increase in fluence generally results in an increase in hydrogen that makes it difficult to separate the effects of these two parameters. If hydrogen were to have an effect it would be expected to increase the yield stress but Figure 7 does not show an increase in yield stress with increasing hydrogen. However, the model does show that yield stress is overpredicted by a small amount on average when excess hydrogen exceeds 600 ppm based on the small amount of data available. Examination of these data shows the uniform elongation strains were very love for these cladding samples suggesting that the decrease is due to embrittlement and not due to elastic-plastic deformation.

Figure 6 shows the predicted minus measured yield stress as a function of temperature. It can be seen from this figure that there is considerable data at room temperature (300K) and between 560 K and 700 K, but very little data between 300 K and 560 K. The model predicts the limited data between 300 K and 560 K well, but more data is needed to better characterize this temperature range.

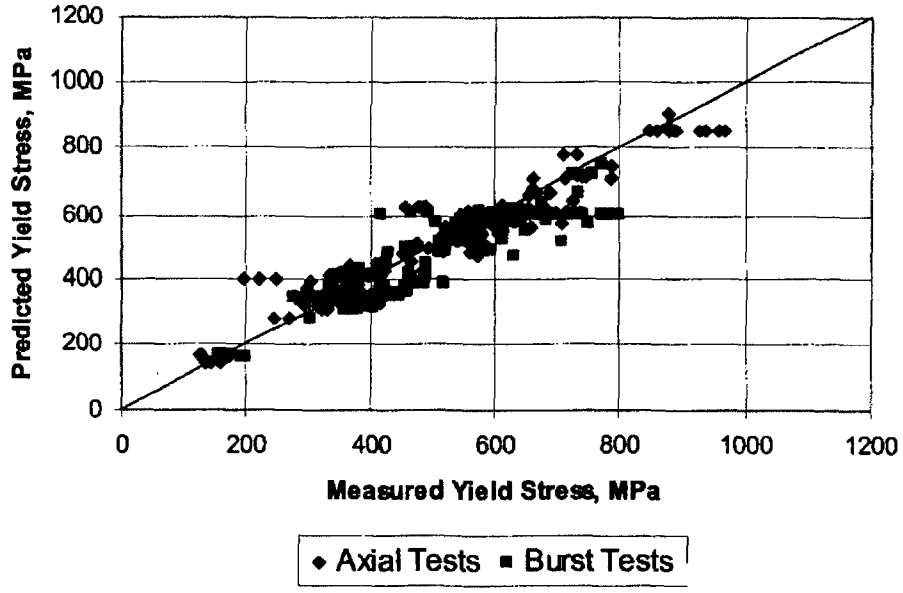

Figure 2: Predicted vs. measured yield stress from the PNNL database

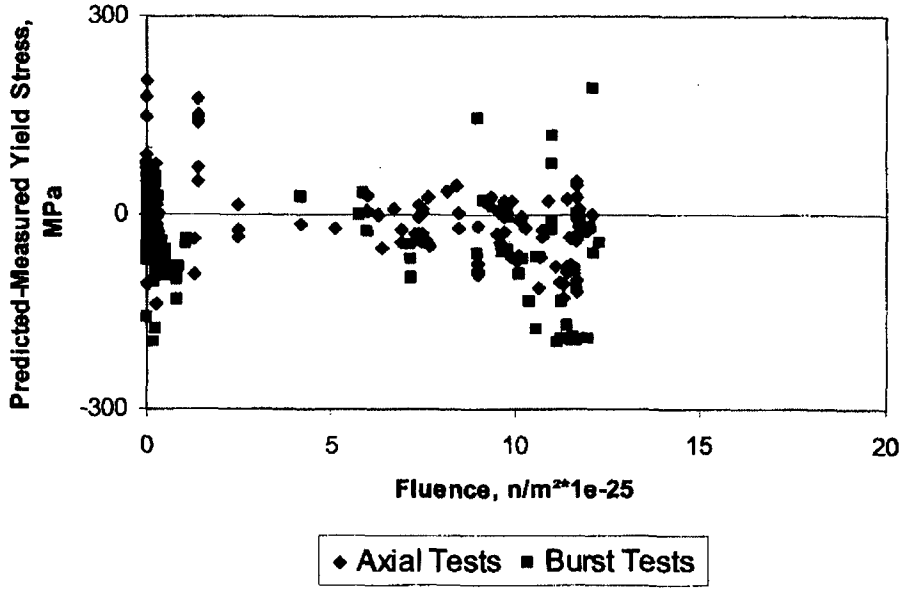

Figure 3: Predicted minus measured yield stress from the PNNL database as a function of fluence.

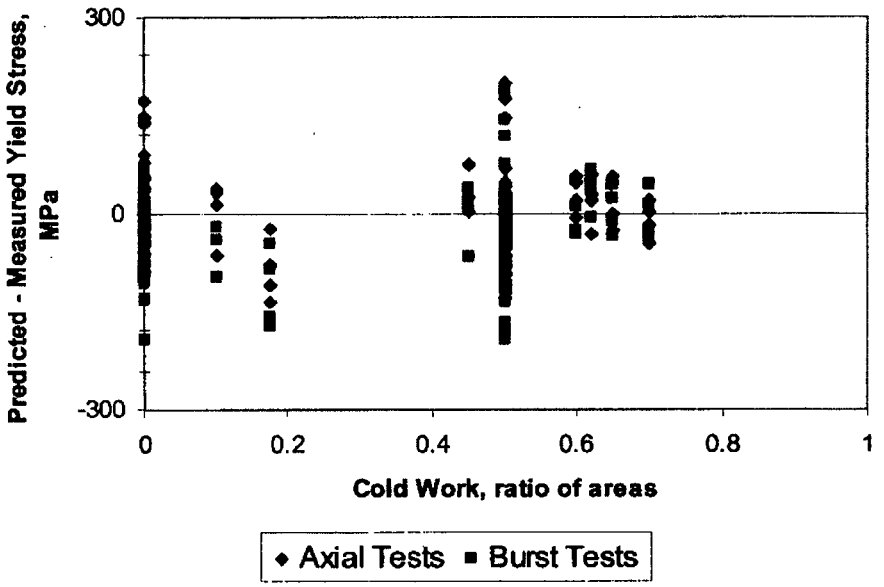

Figure 4: Predicted minus measured yield stress from the PNNL database as a function of cold work.

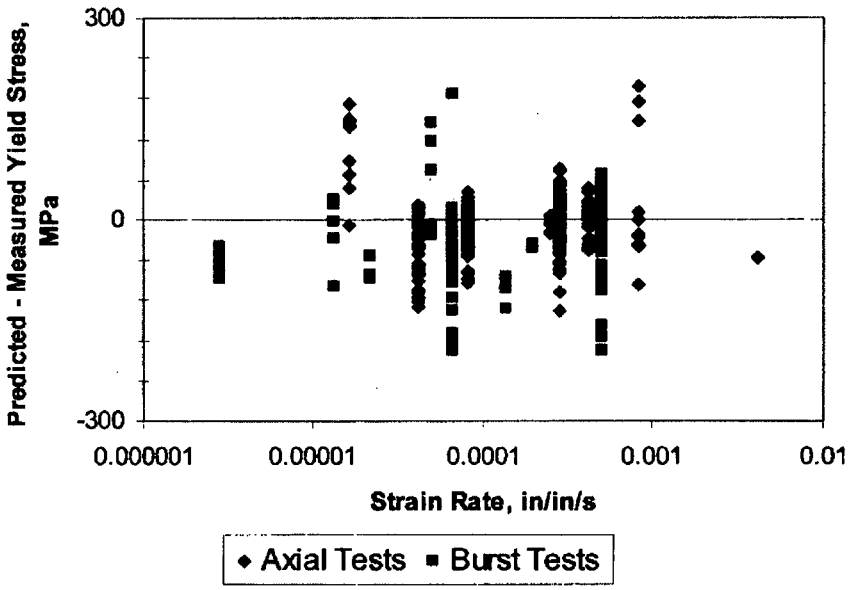

Figure 5: Predicted minus measured yield stress from the PNNL database as a function of strain rate.

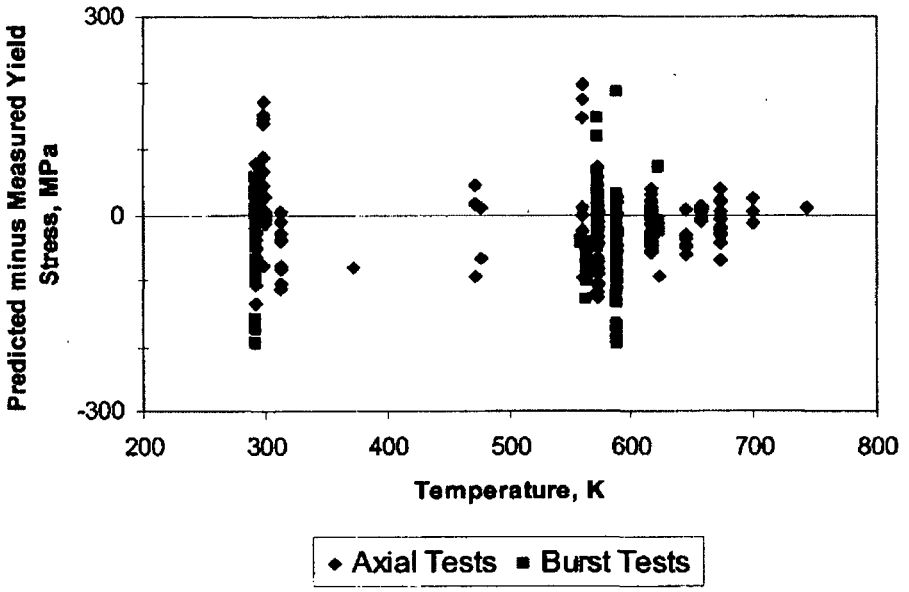

Figure 6: Predicted minus measured yield stress from the PNNL database as a function of temperature.

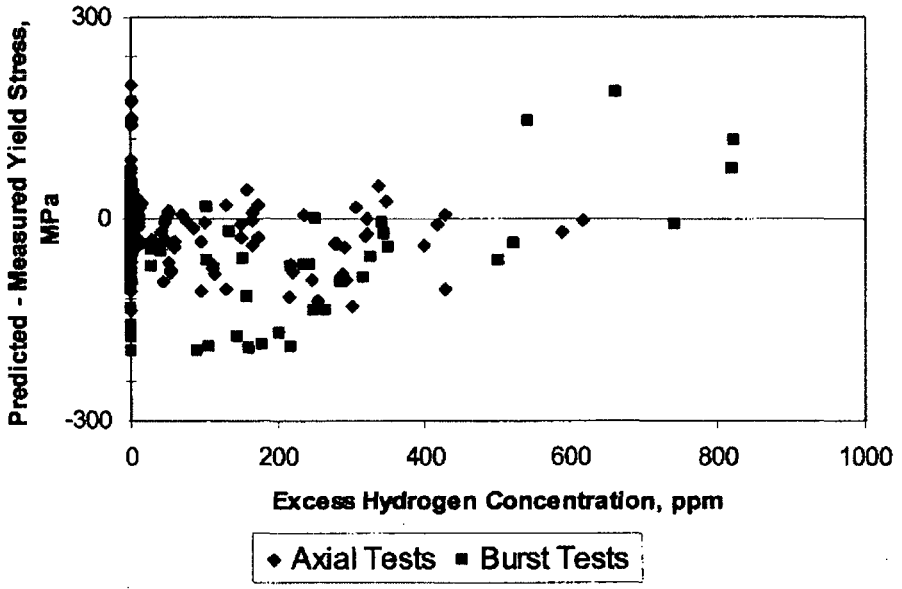

Figure 7: Predicted minus measured yield stress from the PNNL database as a function of excess hydrogen.

Figure 8 shows the PROMETRA data (as displayed in Reference 25) from ring (hoop) and axial tensile tests performed by CEA in France, and the new model predictions for several different strain rates. The actual cold work and fluence values for the samples in the PROMETRA database were not given so a value of 50% was assumed for the cold work and a value of 8×10^{25} n/m^2 was assumed for fluence. The fluence for the data

shown in Figure 8 ranges from $6x10^{25}$ to $12x10^{25}$ n/m² as reported in Reference 25. From this figure it can be seen that the model predicts the data well as a function of temperature and strain rate.

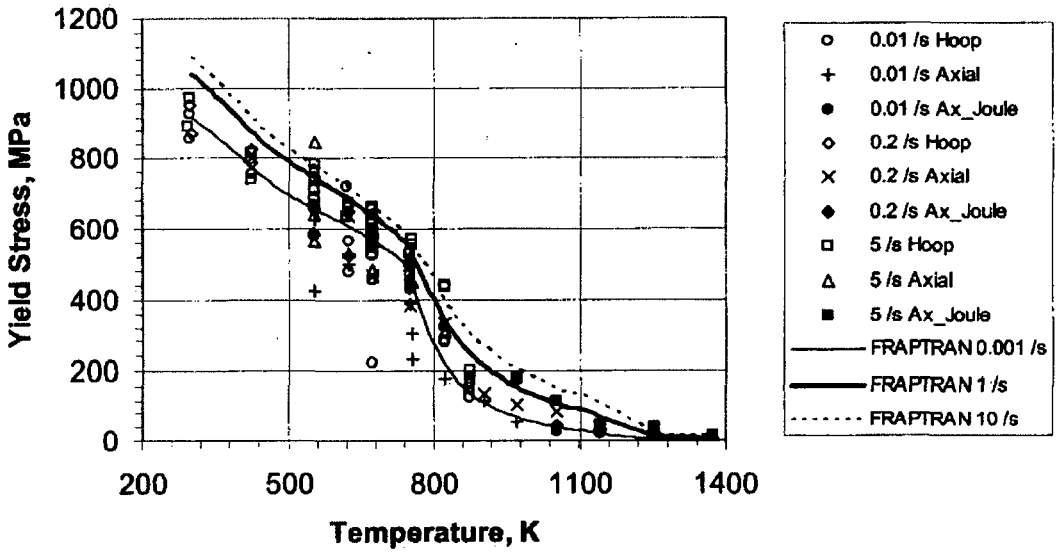

Figure 8: Predicted and measured yield stress from the PROMETRA database as a function of temperature

3.2 Ultimate Tensile Strength

Figure 9 shows a plot of predicted ultimate tensile strength vs. measured ultimate tensile strength for burst tests and axial tension tests from the PNNL database. It can be seen from this figure that the model predicts the data quite well. Generally the upper and lower bound in such ultimate tensile strength data is ±140 MPa, while the model standard error is 71 MPa. It is expected that there will be greater uncertainty in the predictions of ultimate tensile strength than yield strength, since the calculation of ultimate tensile strength is based on both the calculation of yield stress and the calculation of uniform elongation.

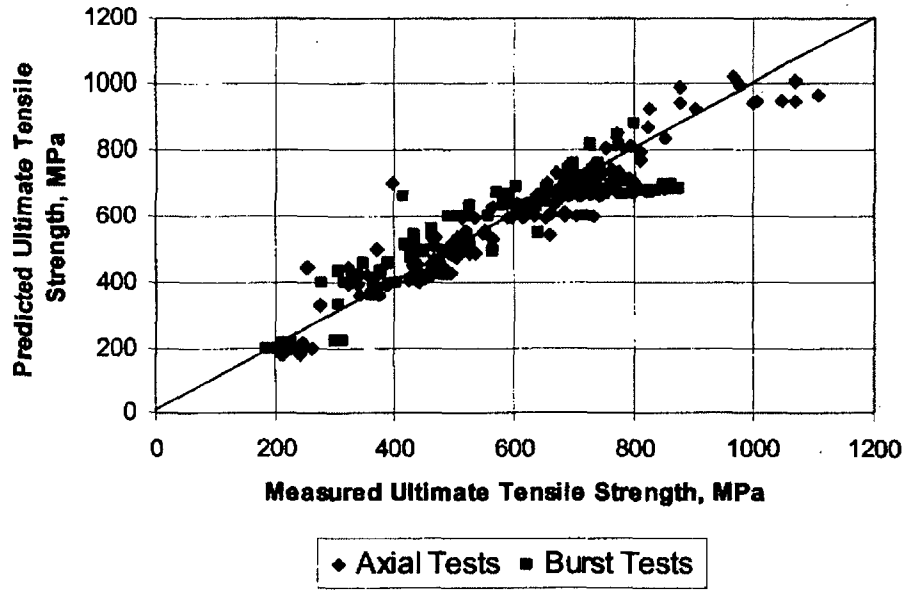

Figure 9: Predicted vs. measured ultimate tensile strength from the PNNL database

Figures 10, 11, 12, 13, and 14 show the predicted minus measured values for the PNNL database as a function of fluence, cold work, strain rate, temperature, and hydrogen concentration, respectively. It can be seen from these figures that there is no apparent bias as a function of fluence, cold work, strain rate, or temperature. There appeas to be a small overprediction in ultimate tensile strength when excess hydrogen exceeds 600 ppm that may be due to the cladding embrittlement as discussed in Section 3.1 for yield stress.

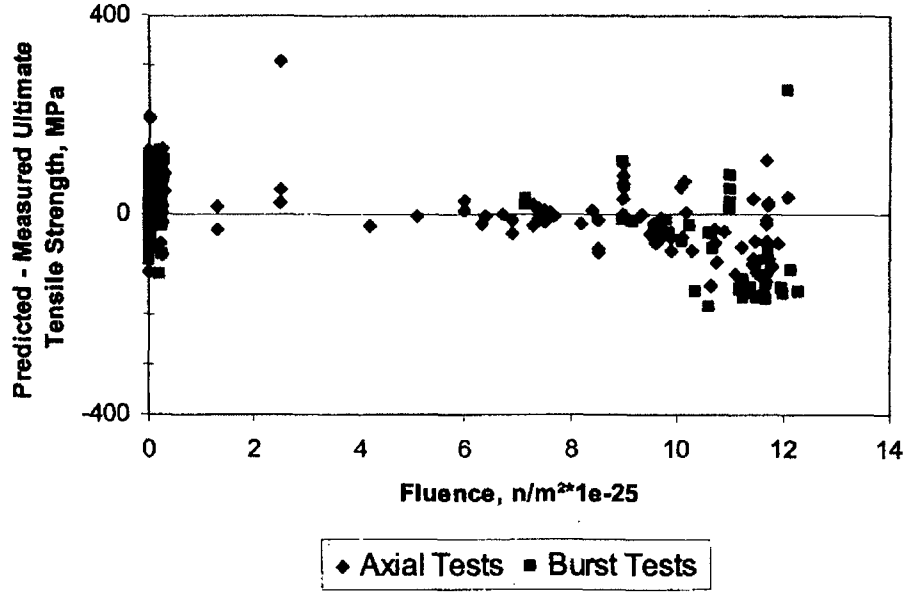

Figure 10: Predicted minus measured ultimate tensile strength from the PNNL database as a function of fluence.

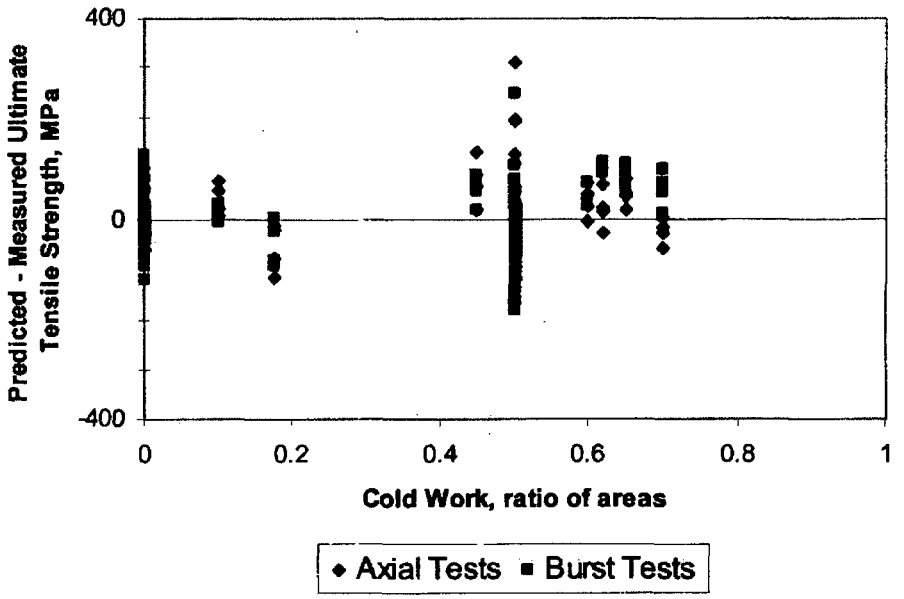

Figure 11: Predicted minus measured ultimate tensile strength from the PNNL database as a function of cold work.

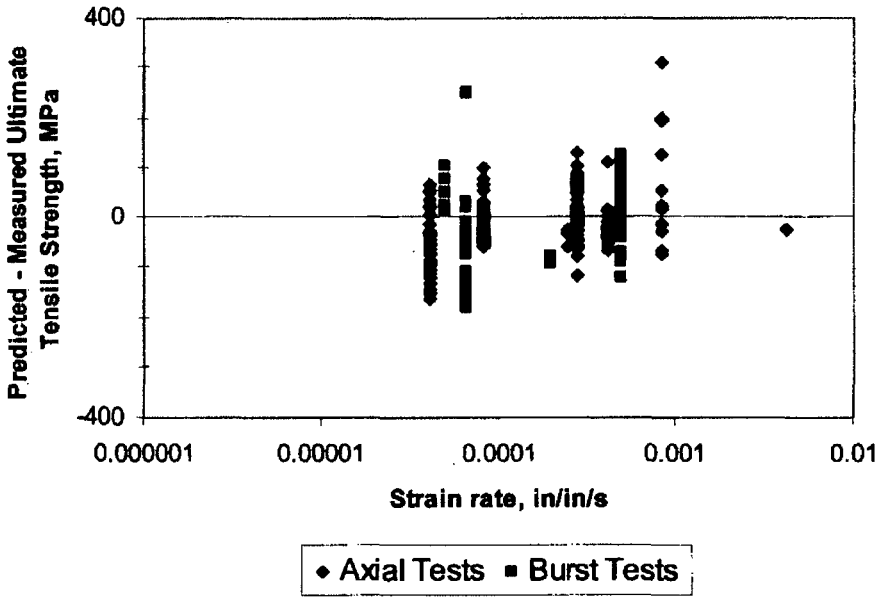

Figure 12: Predicted minus measured ultimate tensile strength from the PNNL database as a function of strain rate.

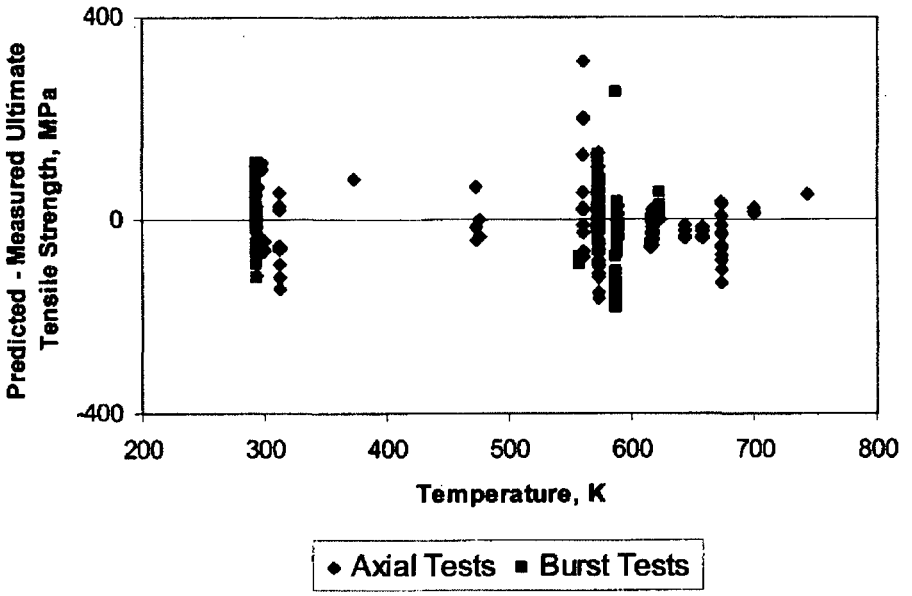

Figure 13: Predicted minus measured ultimate tensile strength from the PNNL database as a function of temperature.

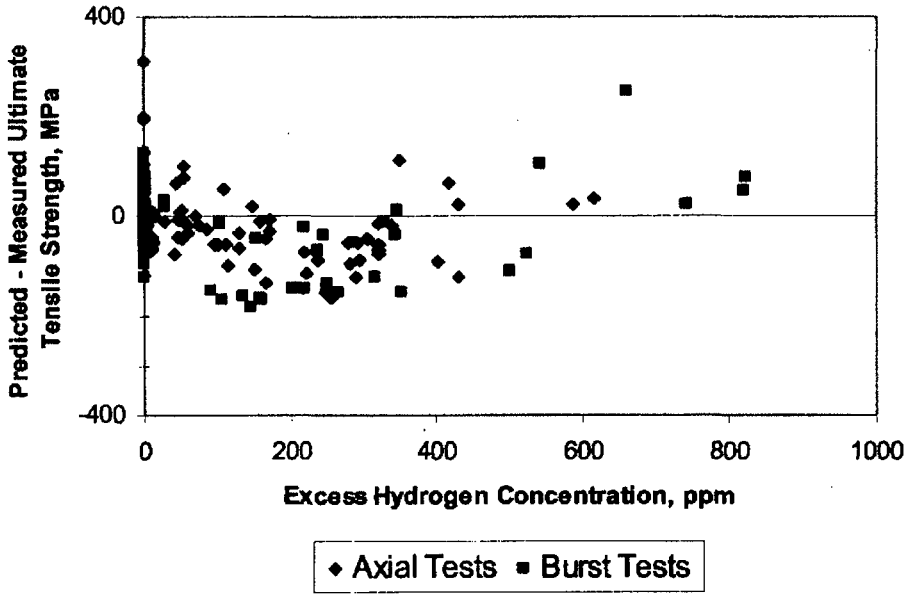

Figure 14: Predicted minus measured ultimate tensile strength from the PNNL database as a function of excess hydrogen concentration.

3.3 Uniform elongation

The predicted vs. measured uniform elongation are shown in Figure 15 for all of the irradiated data in the PNNL database. It can be seen from this figure that there exists a greater degree of scatter in these data than in the YS and UTS data. Most of the scatter at

2.2% predicted uniform elongation comes from cladding with very little total (approximately zero excess) hydrogen concentration that is not characteristic of moderate or high burnup cladding. The predicted minus measured values of uniform elongation from the irradiated samples in the PNNL database are shown in Figures 16 and 17 as a function of excess hydrogen and temperature, respectively. Excess hydrogen is defined as the hydrogen content above the solubility limit which is not dissolved in the matrix, i.e. excess hydrogen equals total hydrogen minus hydrogen dissolved in the matrix. It can be seen from these figures that the new model predicts the uniform elongation to within ±1%. The standard error is 0.9% strain. Figure 16 also demonstrates that the most scatter is seen in the uniform elongation when there is little or no excess hydrogen that is not characteristic of moderate or high burnup cladding..

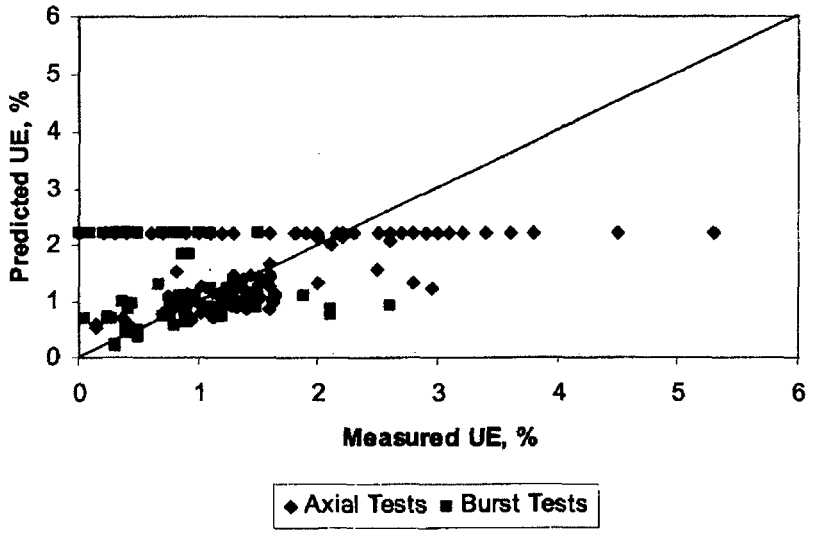

Figure 15: Predicted minus measured uniform elongation from irradiated samples from the PNNL database as a function of excess hydrogen.

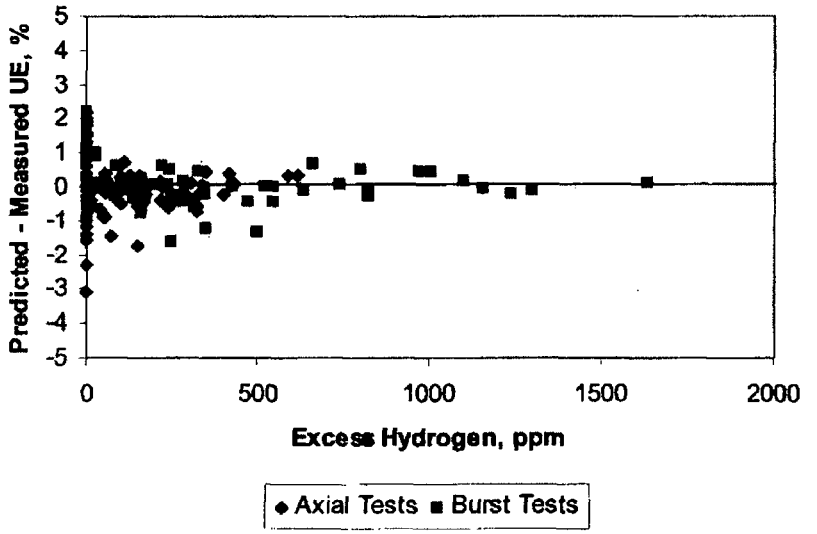

Figure 16: Predicted minus measured uniform elongation from irradiated samples from the PNNL database as a function of excess hydrogen.

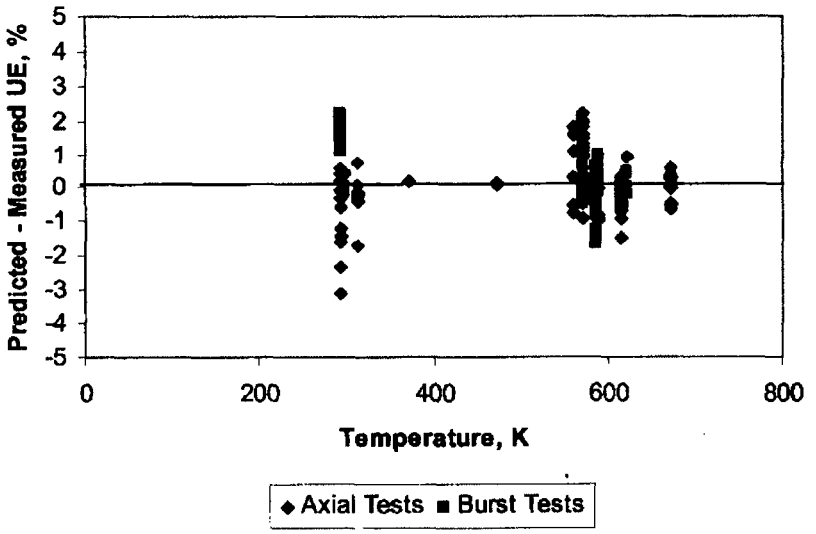

Figure 17: Predicted minus measured uniform elongation from irradiated samples from the PNNL database as a function of temperature.

3.4 Stress vs. Strain Curves

One of the reports from the PNNL database of Zircaloy mechanical properties[9] contained four examples of measured stress vs. strain curves from uniaxial tube tensile tests. These curves were compared to the stress vs. strain curve using the power law that has been adjusted to fit the yield stress and ultimate tensile strength values in the PNNL database.

It should be noted that the measured stress vs. strain curves are engineering stress and strain, while the predicted curves are true stress and strain. Below the uniform elongation, there is little reduction of area, therefore, theoretically these two quantities should be very close. At higher strain values, necking begins and reduction of area causes a large difference between engineering stress and strain and true hoop stress and strain. It is not possible to calculate the true stress from the load vs. displacement data because reduction of area is not measured as a function of displacement. It would be possible to make this measurement, but it has not been made for the data contained in the PNNL database. Because of this, the data and predictions will only be compared up to the uniform elongation value.

Figures 18 - 21 show the measured and predicted stress vs. strain curves, for axial tube tension samples taken at three different temperatures. The solid line in this figure is the model prediction, the dotted line is the measured stress/strain curve calculated from the load vs. displacement measurement, and the squares are the measured 0.2% yield stress and stress at maximum load (UTS).

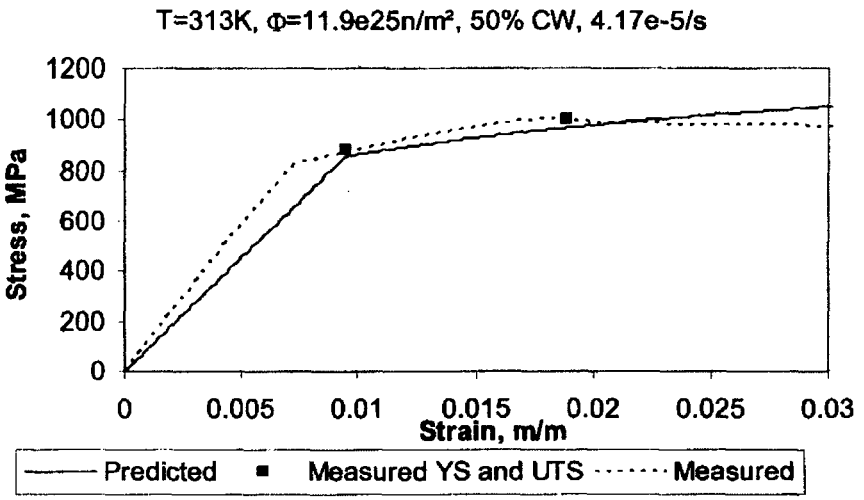

Figure 18: Stress vs. strain curves for uniaxial tube sample (PWR) taken at 313K (40°C)

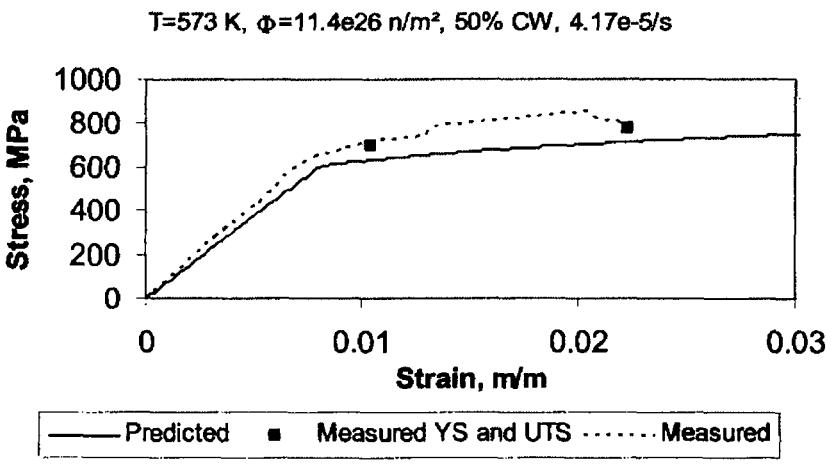

Figure 19: Stress vs. strain curves for uniaxial tube sample (PWR) taken at 573K (300°C)

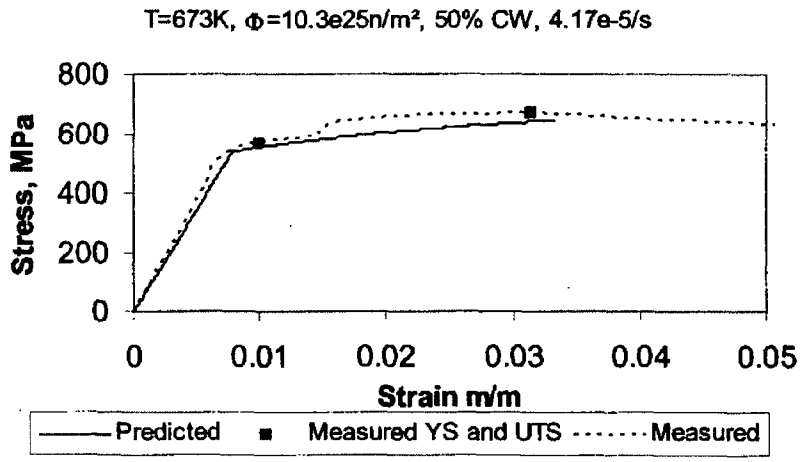

Figure 20: Stress vs. strain curves for uniaxial tube sample (PWR) taken at 673K (400°C)

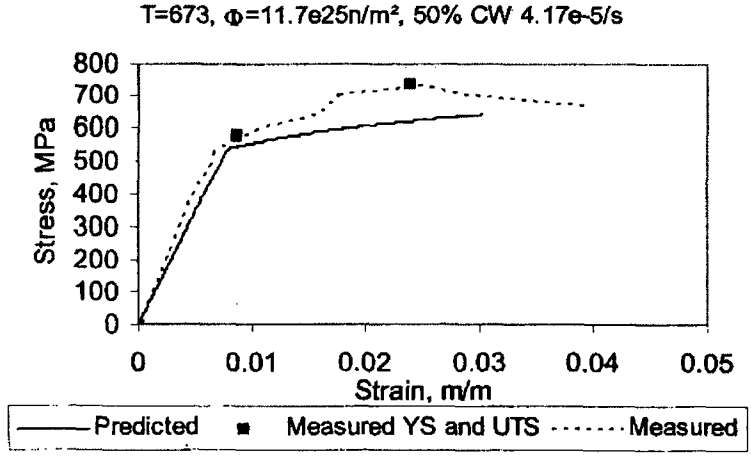

Figure 21: Stress vs. strain curves for uniaxial tube sample (PWR) taken at 673K (400°C)

It can be seen from these figures that the power law with the new mechanical model fitted parameters predicts these four curves reasonably well for PWR-type cladding (cold worked stress relieved). The largest discrepancy comes in Figure 21. However, it should be noted that the conditions for the tests in Figures 20 and 21 are identical, and the model predicts the test in Figure 20 reasonably well. This demonstrates that there is some degree of scatter in this data.

3.5 Ring Stretch Tests

Figures 22 and 23 show predicted vs. measured yield stress and ultimate tensile strength for all the data from the PNNL database including the ring stretch tests. The data from these tests were not used to develop this model, but in comparing them to the new model

it can be seen that the new model predicts these yield and ultimate tensile data as well as the data from the axial tension test and the biaxial burst tests. The scatter in this data is about the same as the scatter in the other data sets. The standard deviation for yield stress including the axial tension tests, biaxial burst tests, and ring stretch tests is 67 MPa, which is about the same as the standard deviation for only the axial tension tests and biaxial burst tests. The standard deviation for ultimate tensile strength including the axial tension tests, biaxial burst tests, and ring stretch tests is 70 MPa, which is slightly lower than the standard deviation for only the axial tension tests and biaxial burst tests. Based on this comparison it appears that the ring stretch tests are as accurate for determining yield stress and ultimate tensile strength as axial tension tests and biaxial burst tests.

Figure 24 shows the predicted minus measured uniform elongation from irradiated cladding as a function of excess hydrogen for all the data from the PNNL database including the ring stretch tests. It can be seen from this figure that the strain data from ring stretch tests displays larger strains than the strain data from axial tension tests or biaxial burst tests. This higher uniform elongation strains measured in the ring tests are attributed to the large bending stress and strains of the ring specimens when plastic deformation is experienced. For this reason, the strain data from the ring stretch tests were not included in the uniform elongation model development.

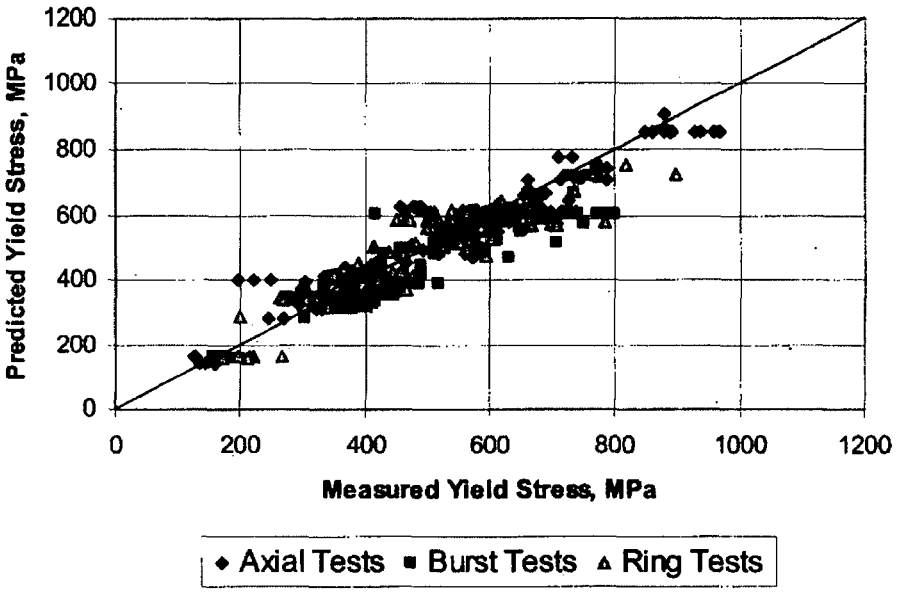

Figure 22: Predicted vs. measured yield stress from the PNNL database

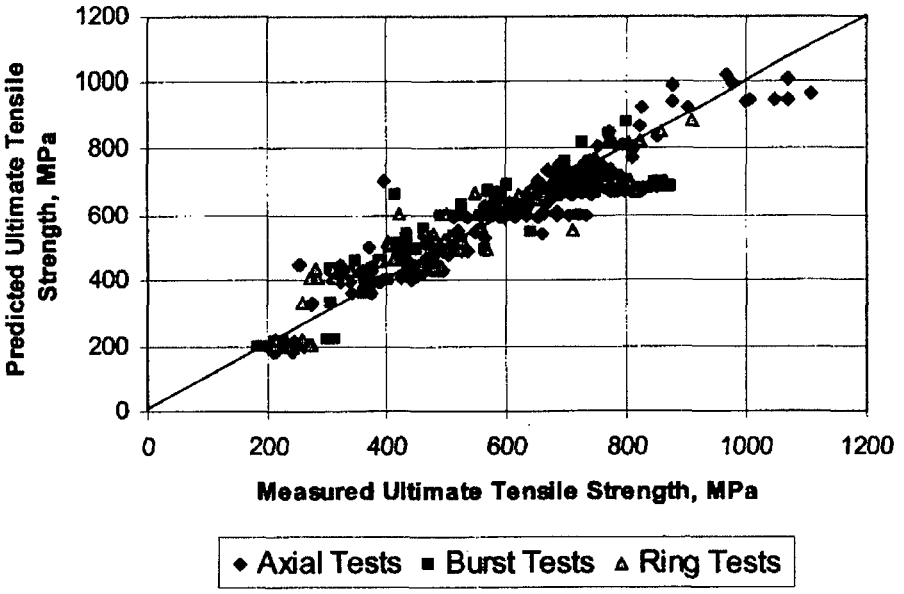

Figure 23: Predicted vs. measured ultimate tensile strength from the PNNL database

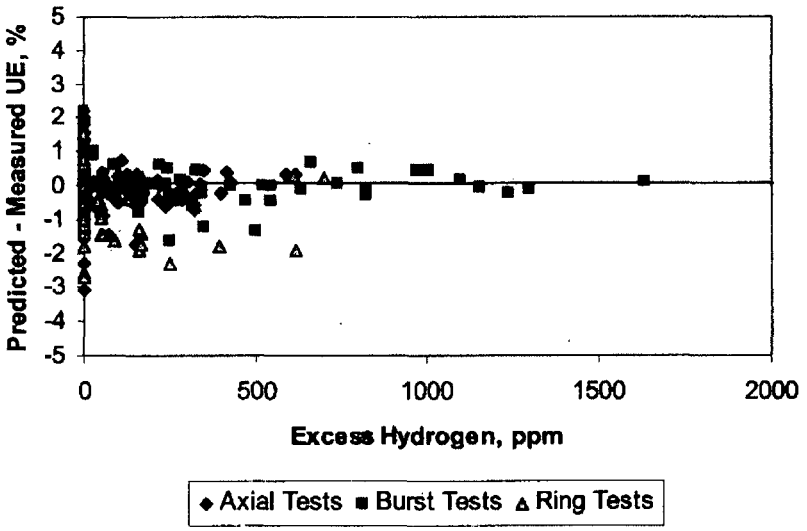

Figure 24: Predicted minus measured uniform elongation from irradiated cladding as a function of excess hydrogen from the PNNL database

3.6 Recrystallized data

The data comparisons shown above are for cold worked, stress relief annealed (SRA) and fully recrystallized (RXA) Zircaloy-4 and Zircaloy-2. However, if only the RXA data is examined it is apparent that while the model predicts the RXA data well, there is a distinct lack of RXA data at high fluence and high hydrogen level. Mechanical data from RXA cladding is important in order to accurately model BWR cladding performance at high burnup.

Figure 25 shows the predicted minus measured yield stress as a function of fast neutron fluence for RXA cladding. The lack of high fluence data can be seen in this figure. Figure 26 shows the predicted minus measured uniform elongation as a function of excess hydrogen concentration for RXA cladding. It can be seen that there is very little data from RXA cladding at high hydrogen concentration. Figure 27 shows the predicted minus measured uniform elongation as a function of temperature concentration for RXA cladding. It can be seen that although these data bound the temperature range of the database, there is relatively little data available for recrystallized cladding.

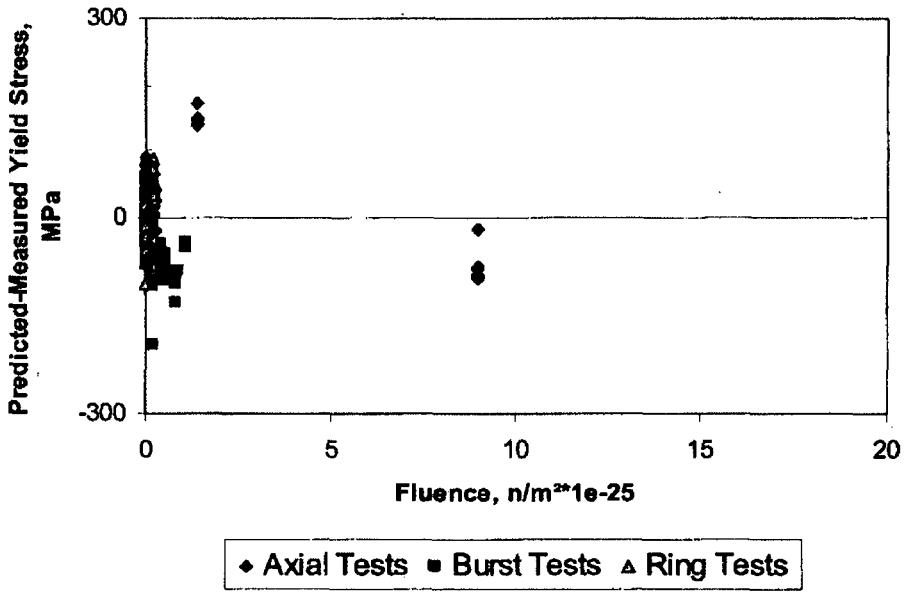

Figure 25: Predicted minus measured yield stress from RXA cladding as a function of fluence

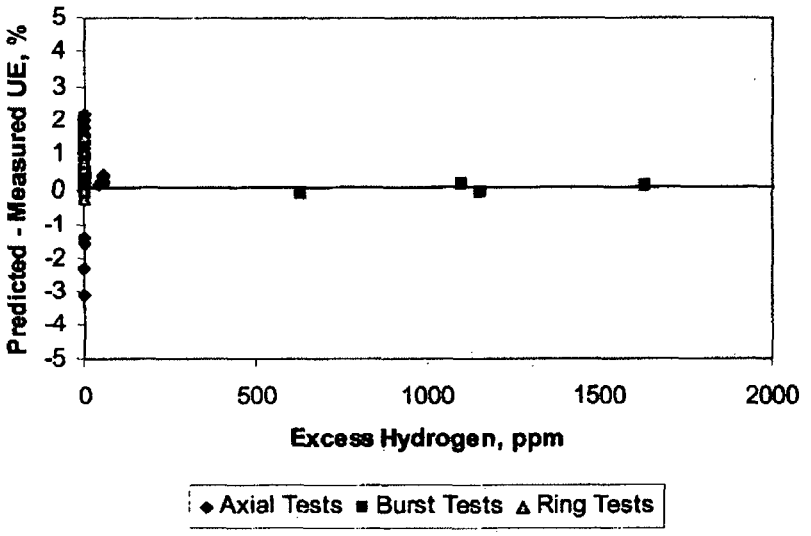

Figure 26: Predicted minus measured uniform elongation from RXA cladding as a function of fluence

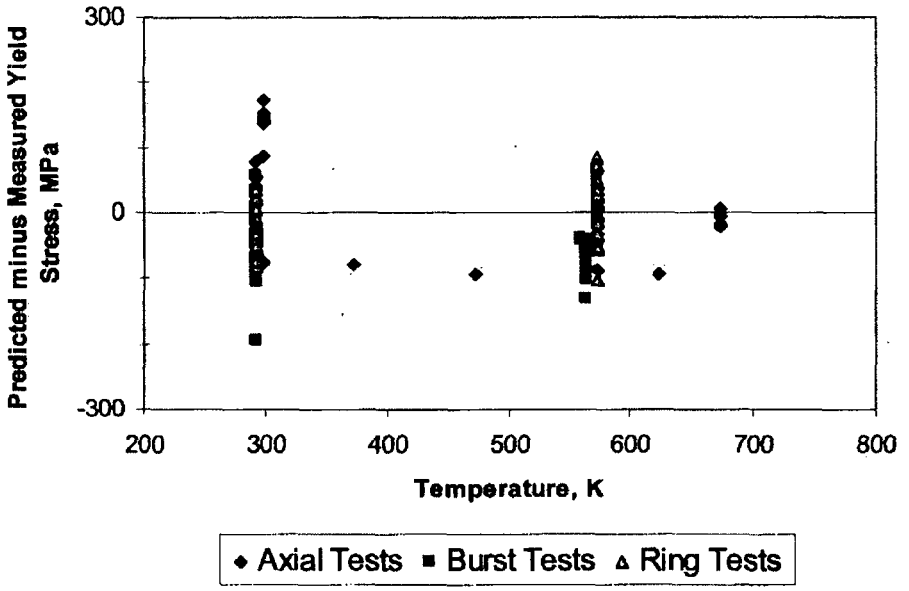

Figure 27: Predicted minus measured uniform elongation from RXA cladding as a function of temperature

4 Recommendations for Modeling Spent Fuel Cladding

Certain assumptions about what the condition of fuel rods being modeled in spent fuel casks must be made in order to correctly model their behavior in accident situations. This section will discuss what PNNL's recommendations are for modeling spent fuel cladding from PWRs and BWRs.

Table 1 list the recommended fast neutron fluence, cladding type, cold work, and hydrogen concentration for PWR and BWR cladding that should be used for spent fuel accident analyses at high burnup (50 to 60 GWd/MTU). These values are estimated to be the mean rod average of discharged high burnup fuel rods with Zircaloy-4 (PWR) and Zircaloy-2 (BWR) cladding. The two variables that are omitted from this table that can affect the cladding properties are the temperature and the strain rate. These variables will be defined in the accident analysis.

Table 1: Recommended fast neutron fluence, cladding type, hydrogen concentration, and cold work for PWR and BWR cladding under spent fuel conditions

	PWR	**BWR**
Fast neutron fluence	1.2×10^{26} n/m^2	1.2×10^{26} n/m^2
Cladding type	Zircaloy-4	Zircaloy-2
Cladding cold work	50%	0%
Hydrogen concentration	500 ppm	250 ppm

In order to show the effect that each of these parameters has on the yield stress, ultimate tensile strength, and the uniform elongation, each of these parameters has been plotted as a function of each variable that it is dependant upon while holding the other variables constant at recommended values. Figures 28, 29, 30, and 31 show the predicted yield stress for PWR and BWR conditions as a function of temperature, fast neutron fluence, cold work and strain rate, respectively.

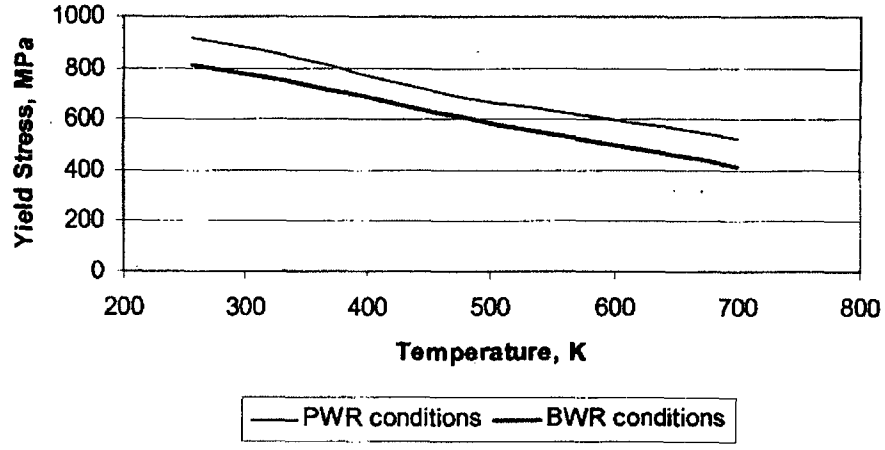

Figure 28: Model predictions of yield stress for PWR (CWSRA ZR-4) and BWR (RXA Zr-2) conditions as a function of temperature for strain rate of 1×10^{-4} in/in/s.

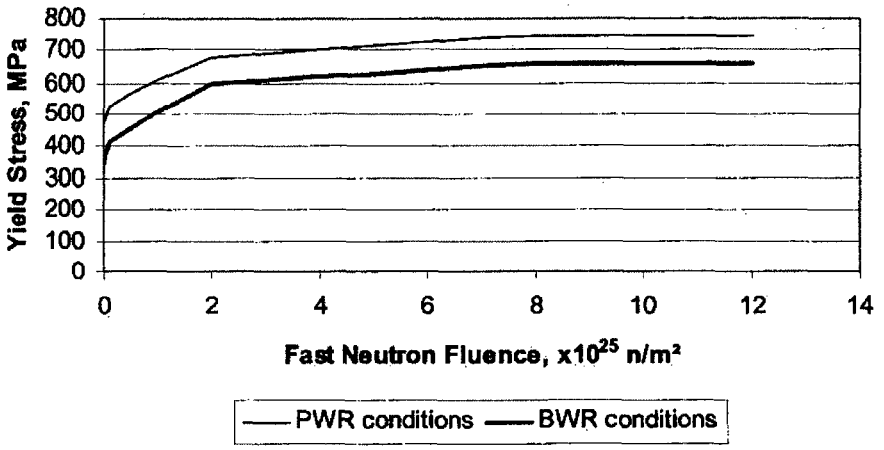

Figure 29: Model predictions of yield stress for PWR (CWSRA Zr-4) and BWR (RXA Zr-2) conditions as a function of fast neutron fluence for temperature of 300°F and strain rate of $1x10^{-4}$ in/in/s.

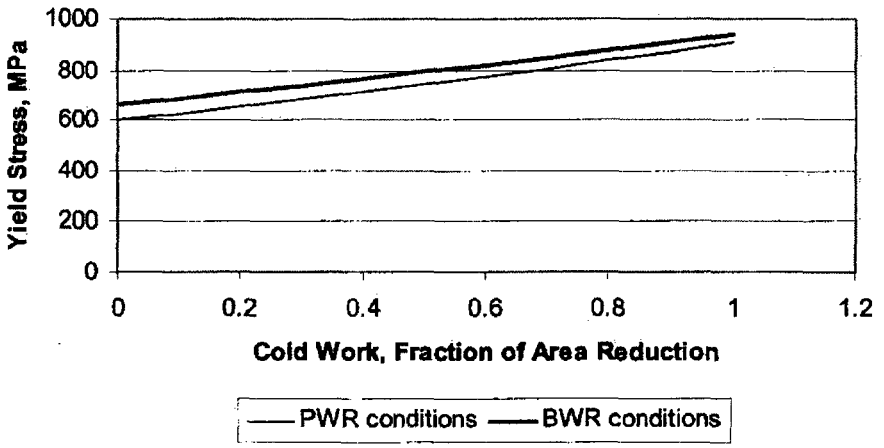

Figure 30: Model predictions of yield stress for PWR (CWSRA ZR-4) and BWR (RXA Zr-2) conditions as a function of cold work for temperature of 300°F and strain rate of $1x10^{-4}$ in/in/s.

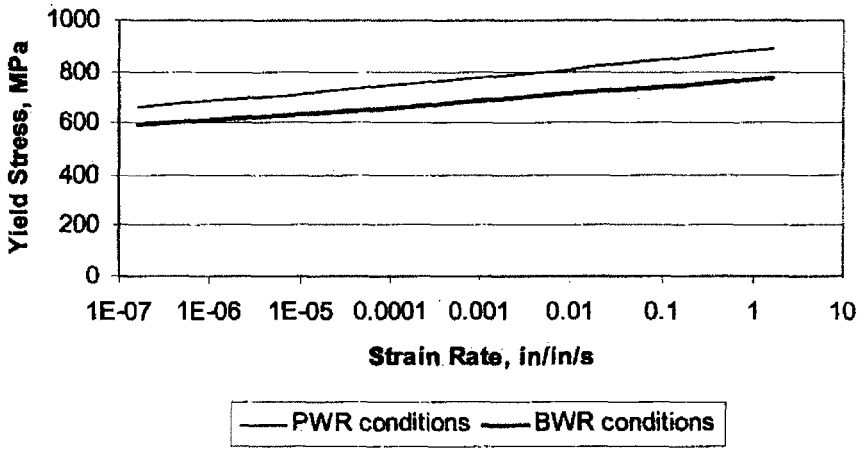

Figure 31: Model predictions of yield stress for PWR and BWR conditions as a function of strain rate for temperature of 300°F.

Figures 32, 33, 34, 35, and 36 show the predicted ultimate tensile strength for PWR and BWR conditions as a function of temperature, fast neutron fluence, cold work, strain rate, and excess hydrogen, respectively.

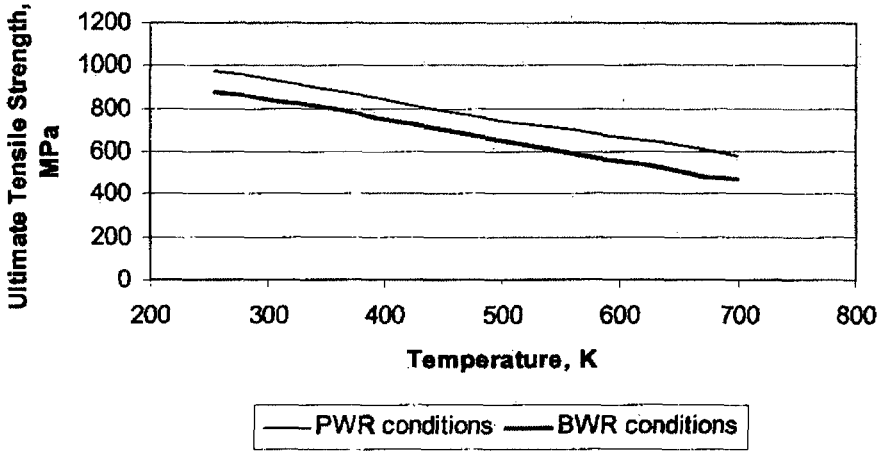

Figure 32: Model predictions of ultimate tensile strength for PWR and BWR conditions as a function of temperature for strain rate of $1x10^{-4}$ in/in/s.

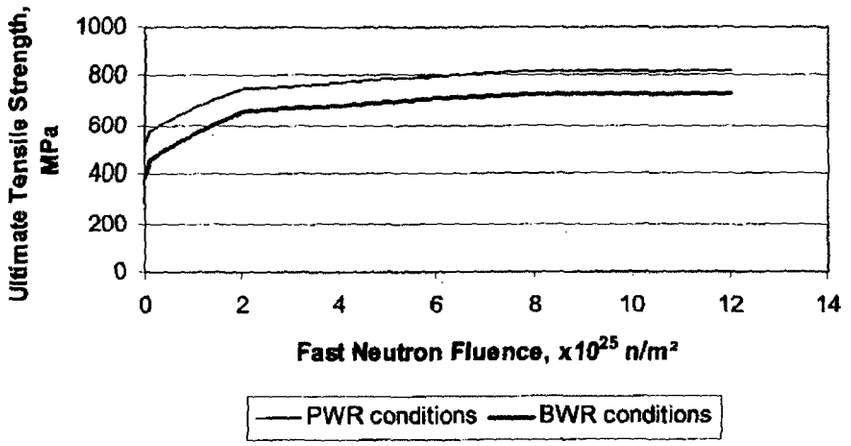

Figure 33: Model predictions of ultimate tensile strength for PWR and BWR conditions as a function of fast neutron fluence for temperature of 300°F and strain rate of $1x10^{-4}$ in/in/s.

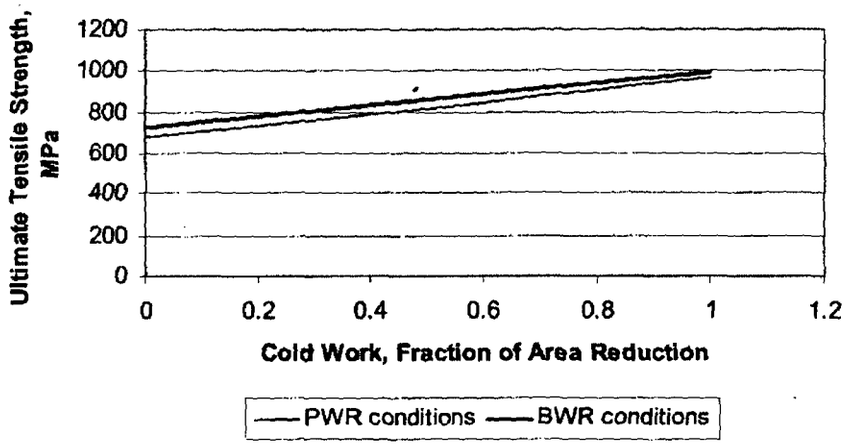

Figure 34: Model predictions of ultimate tensile strength for PWR and BWR conditions as a function of cold work for temperature of 300°F and strain rate of $1x10^{-4}$ in/in/s.

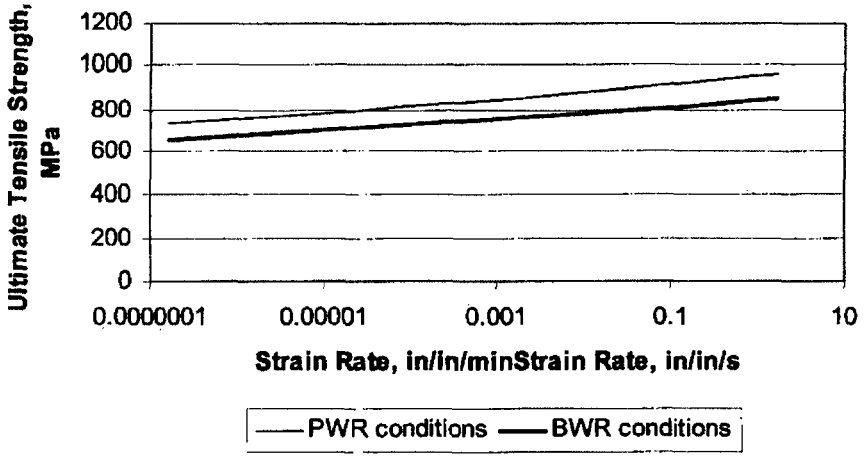

Figure 35: Model predictions of ultimate tensile strength for PWR and BWR conditions as a function of strain rate for temperature of 300°F.

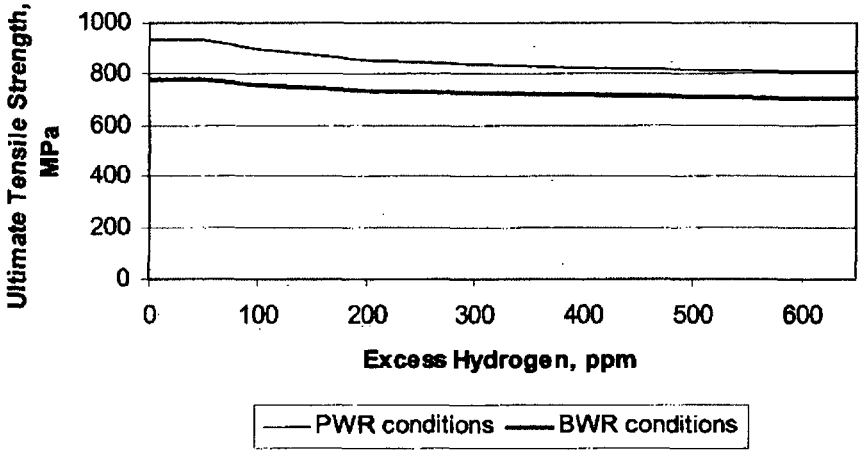

Figure 36: Model predictions of ultimate tensile strength for PWR and BWR conditions as a function of excess hydrogen for temperature of 300°F and strain rate of $1x10^{-4}$ in/in/s.

Figures 37 and 38 show the predicted uniform elongation for PWR and BWR conditions as a function of temperature and excess hydrogen, respectively. It should be noted that uniform elongation is not shown versus strain rate because this data is not currently available at high strain rate, i.e. > $1x10^{-3}$ in/in/s. It is anticipated that there may be a decrease in uniform and total elongation at high strain rate because both yield and ultimate strength are shown to increase by 15 to 20% between strain rates of 10^{-3} in/in/s and 1in/in/s. This is because increases in Zircaloy cladding strength due to flounce and cold work both result in significant decreases in strain with total elongation having the largest decrease.

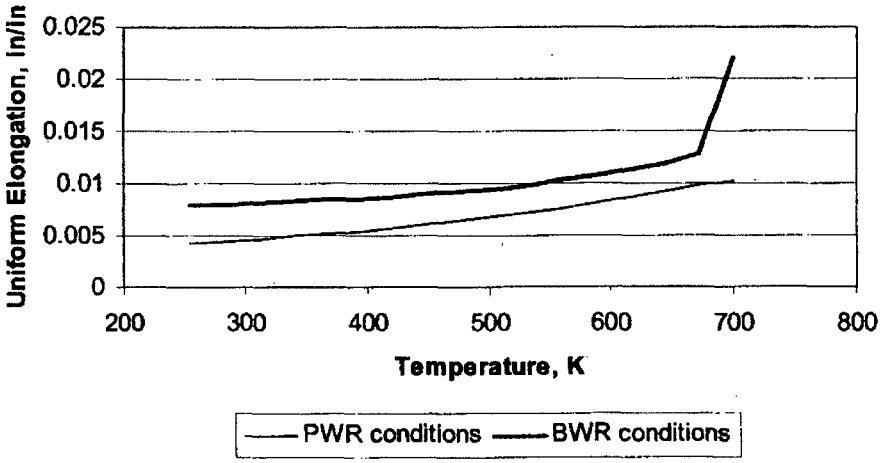

Figure 37: Model predictions of uniform elongation for PWR and BWR conditions as a function of temperature for strain rate of $1x10^{-4}$ in/in/s.

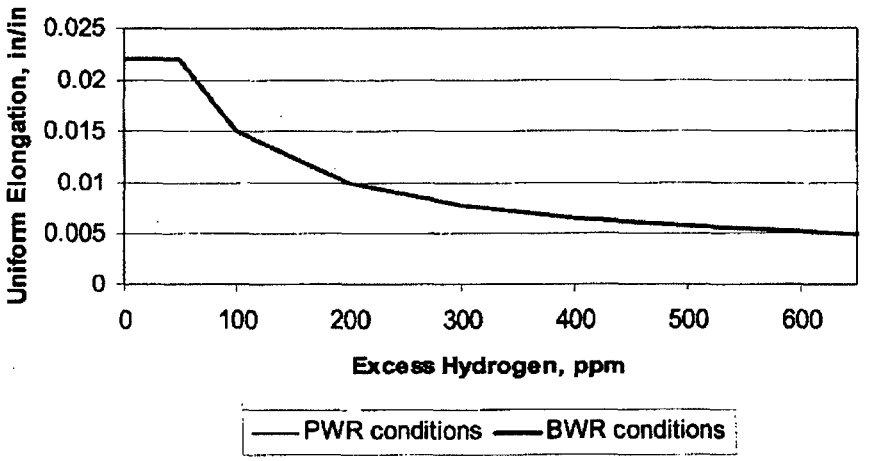

Figure 38: Model predictions of uniform elongation for PWR and BWR conditions as a function of excess hydrogen for temperature of 300°F and strain rate of $1x10^{-4}$ in/in/s.

5 Future Work

As more data become available, such as from the ANL mechanical test program, our knowledge of the stress strain behavior of Zircaloy will be expanded. New data that fall outside of the regimes (e.g., of fluence, strain rate, hydrogen and temperature) where we currently have data will either confirm our assumptions for modeling, or give us new insights that allow us to adjust the model to better predict the stress/strain behavior in those regimes.

New data that are taken in operating regimes where data is already available will either confirm the data existing in the current database, or if it does not agree the uncertainty of the model will increase. If the later occurs, PNNL will critically examine both the new data and the old data, and determine if such things as test specimen design or material

non-uniformities can explain the difference. If so, then PNNL will use the data from the test specimens closest to the geometry that will be seen in reactor or in spent fuel conditions to update the model if necessary. Two papers have recently been discovered that offer explanations why differences in measured strain can occur due to specimen geometry. The first paper[29] describes a difference in measured strain as a function of gage length in irradiated materials that deform by dislocation channeling, as Zircaloy does. The second paper[30] describes how the gage width to thickness ratio can affect the measured strain. Papers like these and possibly others may be used to reconcile differences in mechanical property measurements as new data are collected.

Mechanical properties at high strain rate 0.01 to 10 /s are needed to be prototypic of deformation rates in cask accidents to model uniform and total strains and verify the yield stress dependence observed in the French PROMETRA tests performed by CEA. The current mechanical database for U.S. fabricated cladding has a strain rate between $2x10^{-6}$ to $4x10^{-3}$ /s. Mechanical properties data are needed from BWR cladding (RXA Zr-2) at high fluences (burnup) and hydrogen content to verify the correlations for fully recrystallized Zircaloy-2 at high burnup. In addition, both PWR cold-worked and BWR RXA cladding data are needed from high burnup cladding at temperatures between room temperature and 550K. Currently there is mechanical data to validate the new model at room temperature (300K) and 550K, but because there is little data between these two temperature s, the model is interpolating between this temperature range.

5. Conclusions

A new model for stress/strain behavior in Zircaloy has been developed that adequately predicts the yield stress and ultimate tensile strength under uniaxial conditions for unirradiated and irradiated Zircaloy. This model was developed using axial tension tests and biaxial burst tests, and validated with ring stretch tests. The standard deviation in the difference between the model and the data from the three data sources is 67 MPa and 70 MPa for yield stress and ultimate tensile strength, respectively. In addition, the model adequately predicts the uniform elongation for irradiated Zircaloy. These elastic-plastic models may not be applicable when hydrogen concentrations exceed 650 ppm or when strain rates are high. These conditions can cause brittle fracture and is not considered by these models.

The shape of the predicted stress/strain curve between the yield stress and ultimate tensile strength was compared to several measured stress/strain curves, and was found to reasonably predict the shape of the curve. It should be noted that due to the variation in yield stress, the curve may be shifted up or down, but in general the shape of the predicted stress/strain agrees well with the data.

Possibilities for improving this model exist, and as more data is made available it will be used to verify or change the model where no data currently exist. If data is found that contradicts data that is currently being used in the formulation of this model, all the data will be critically reviewed and the data that comes from tests that best conforms to the geometry and conditions in-reactor will be used to improve the model.

References

1. G. A. Berna et al., "FRAPCON-3: A Computer Code for the Calculation of Steady-State, Thermal-Mechanical Behavior of Oxide Fuel Rods for High Burnup," NUREG/CR-6534, Vol. 1, PNNL-11513, Nuclear Regulatory Commission and Pacific Northwest National Laboratory (1997).

2. M. E. Cunningham el al., "FRAPTRAN: A Computer Code for the Transient Analysis of Oxide Fuel Rods," NUREG/CR-6739 Vol. 1, PNNL-13576, Nuclear Regulatory Commission and Pacific Northwest National Laboratory (2001).

3. A. M. Garde, "Hot Cell Examination of Extended Burnup Fuel From Fort Calhoun," DOE/ET/34030-11, U.S. Department of Energy and Combustion Engineering (1986).

4. M. G. Balfour, "Zorita Research and Development Program Volume 1, Final Report," WCAP-10180, Westinghouse Electric Corporation (1982).

5. C. G. Dideon and G. M. Bain, "Fuel Performance Under Extended-Burnup Operation B&W 15x15 Design," DOE/ET/34212-38, BAW-1716, U.S. Department of Energy and Babcock and Wilcox (1983).

6. L. W. Newman "The Hot Cell Examination of Oconee 1 Fuel Rods after Five Cycles of Irradiation," DOE/ET/34212-50, BAW-1874, U.S. Department of Energy and Babcock and Wilcox (1986).

7. L. W. Newman, "Development of an Extended Burnup Mark B Design," DOE/ET/34213-16, BAW 1532-13, U.S. Department of Energy and Babcock and Wilcox (1990).

8. G. P. Smith, "Hot Cell Examination of Extended Burnup Fuel from Calvert Cliffs-1," TR-103302-V2, ABB Combustion Engineering (1994).

9. G. P. Smith, "The Evaluation and Demonstration of Methods for Improved Nuclear Fuel Utilization, End-of-Cycles 6 and 7 Fuel Examinations," DOE/ET/34010-10, CEND-414, U.S. Department of Energy and C-E Power Systems (1983).

10. L. M. Lowry et al., "Evaluating Strength and Ductility of Irradiated Zircaloy, Task 5," NUREG/CR-1729, BMI-2066 Vol. 1, Nuclear Regulatory Commission and Battelle Columbus Laboratories (1981).

11. A. M. Garde, "Effects of Irradiation and Hydriding on the Mechanical Properties of Zircaloy-4 at High Fluence" *Zirconium in the Nuclear Industry: 8th International Symposium, ASTM STP 1023*, p. 548, American Society for Testing and Materials, Philadelphia, U.S.A. (1989).

12. D. H. Hardy, "The Effect of Neutron Irradiation on the Mechanical Properties of Zirconium Alloy Fuel Cladding in Uniaxial and Biaxial Tests" *Irradiation Effects on Structural Alloys for Nuclear Reactor Applications, ASTM STP 484*, p. 215, American Society for Testing and Materials, Toronto, Canada (1970).

13. A. M. Garde et al., "Effects of Hydride Precipitate Localization and Neutron Fluence on the Ductility of Irradiated Zircaloy-4," *Zirconium in the Nuclear Industry: 11th International Symposium, ASTM STP 1295*, p. 407, American Society for Testing and Materials, Garmisch-Partenkirchen, Germany (1996).

14. R. S. Kemper and D. L. Zimmerman, "Neutron Irradiation Effects on the Tensile Properties of Zircaloy-2," HW-52323, General Electric Company (1957).

15. W. R. Smalley, "Saxton Core II Fuel Performance Evaluation Part I: Materials" WCAP 3385-56 Part 1, Westinghouse Electric Corporation (1971).

16. L. Berat-Robert et al., "Influence of a Zirconia Layer on the Mechanical Behavior of Zircaloy-4 Cladding and Thimble Tubes," *LWR Fuel Performance Meeting*, Vol. 2, p. 931, Park City, USA (2000).

17. R. Chun et al., "Dynamic Impact Effects on Spent Fuel Assemblies" UCID - 21246, Lawrence Livermore National Laboratory (1987).

18. S. T. Mahmood et al., "Effects of SPP Dissolution on Mechanical Properties of Zircaloy-2" *LWR Fuel Performance Meeting*, p. 440, Portland, U.S.A. (1997).

19. M.G Balfour "High Burnup Fuel Rod Hot Cell Program, Vol. 1: Final Report," DOE/ET 34073-1, WCAP-10238, U.S. Department of Energy and Westinghouse Electric Corporation (1982).

20. A. Hermann, "Fuel Cladding Integrity at High Burnups (Part I)," Draft TR-108753-P1, Paul Scherrer Institute Laboratory for Materials Behavior (1999).

21. K. Pettersson et al., "Effect of Irradiation on the Strength, Ductility, and Defect Sensitivity of Fully Recrystalized Zircaloy Tube", *Zirconium in the Nuclear Industry, 4th conference, ASTM STP 681*, p. 155 Stratford-upon-Avon, England (1979).

22. L. F. Van Swan, et al., "Behavior of Zircaloy-4 and Zirconium Liner Zircaloy-4 Cladding at High Burnup," *LWR Fuel Performance Meeting*, p. 421, Portland, USA (1997).

23. S.B. Wisner, R.B. Adamson, "Combined Effects of Radiation Damage and Hydrides on the Ductility of Zircaloy-2," *Nuclear Engineering and Design*, **185,** 33 (1998).

24. M. C. Billone, "The Mechanical Properties Expert Group Update on Round Robin Test Results," Argonne National Laboratory (2002).

25. M. Balourdet et al., "The PROMETRA Programme : assessment of mechanical properties of zircaloy-4 cladding during an RIA," *SMIRT15 – 15th International Conference on Structural Mechanics in Reactor Technology*, Vol. II, p. 485, Seoul, Korea (1999).

26. A. Higdon et al., *Mechanics of Materials, Fourth Edition*, Chapter 9, John Wiley & Sons, New York (1985).

27. D. L. Hagrman et al., "MATPRO – Version 11 (Revision 2) A Handbook of Materials Properties for Use in the Analysis of Light Water Reactor Fuel Rod Behavior," NUREG/CR-0479, TREE-1280, Nuclear Regulatory Commission and EG&G (1981).

28. K. J. Geelhood et al., "Modifications to FRAPTRAN to Predict Fuel Rod Failures Due to PCMI during RIA-Type Accidents," *Proceedings of the 2004 International Meeting on LWR Fuel Performance*, Orlando, USA (2004).

29. R. B. Adamson et at., "Failure Strain for Irradiated Zircaloy Based on Subsized Specimen Testing and Analysis," *The Use of Small Scale Specimens for Testing Irradiated Material*, ASTM STP 888, p. 171 (1986).

30. A. K. Chakrabarti and J. W. Spretnak, "Instability of Plastic Flow in the Directions of Pure Shear: II. Experimental," *Metallurgical Transactions A*, **6A**, 737 (1975).

APPENDIX 2

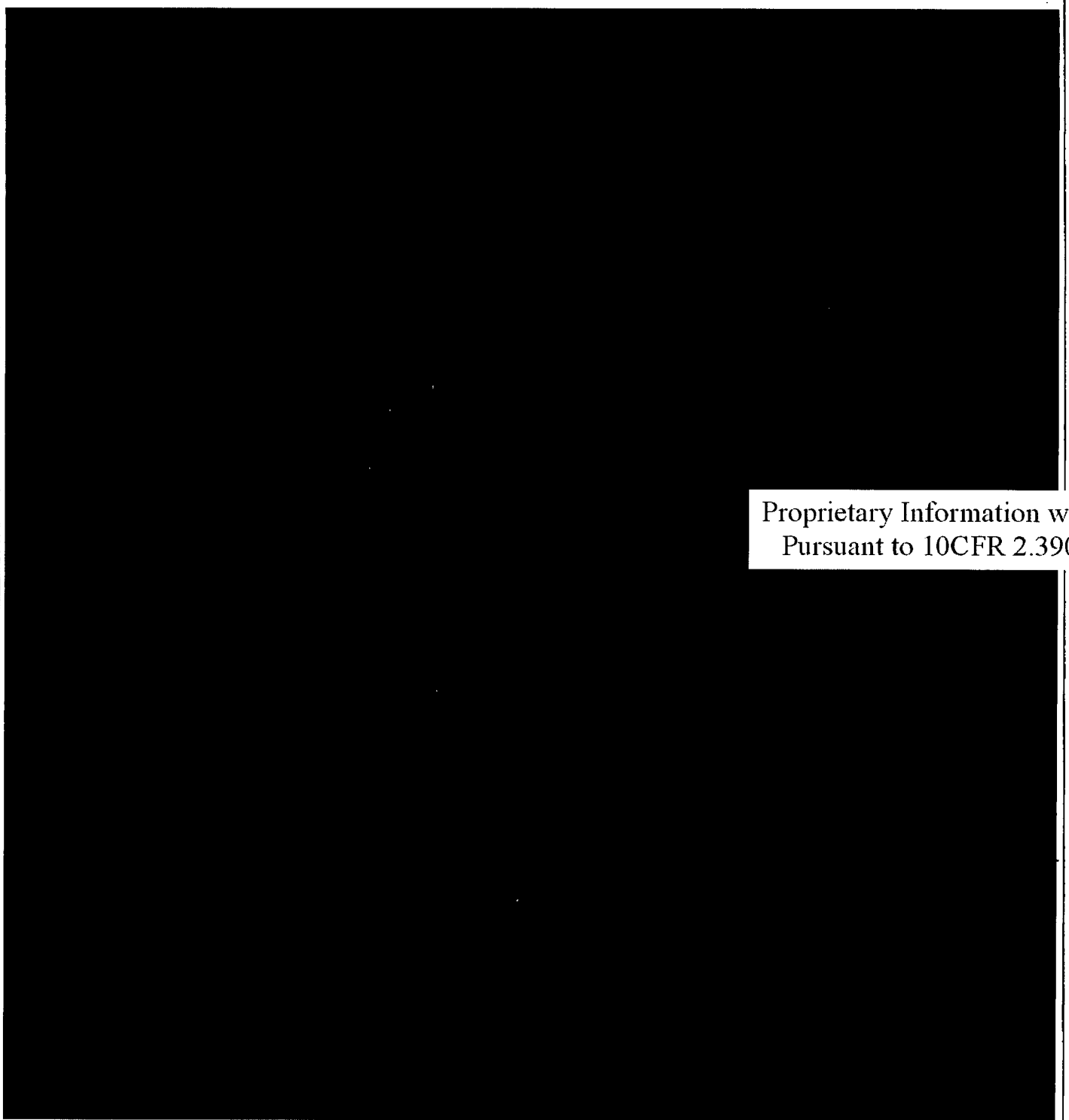

Proprietary Information with
Pursuant to 10CFR 2.390

[redacted]

Proprietary Information with
Pursuant to 10CFR 2.390